

Terahertz response of acoustically driven optical phonons

R. H. Poolman, E. A. Muljarov, and A. L. Ivanov

Department of Physics and Astronomy, Cardiff University, Cardiff CF24 3AA, United Kingdom

(Received 8 April 2010; revised manuscript received 24 May 2010; published 17 June 2010)

The manipulation of transverse-optical (TO)-phonon polaritons and the associated terahertz (THz) light field by means of an ultrasound acoustic wave is proposed and illustrated by calculating the TO-phonon-mediated THz response of acoustically pumped CuCl and TlCl crystals. We show the high-contrast acoustically induced change in the THz reflectivity and multiple THz Bragg replicas, which are associated with the far-infrared-active TO-phonon resonance driven by the ultrasonic wave. The effect, which stems from phonon anharmonicity and deals with the resonantly enhanced acousto-optical susceptibilities, refers to an operating acoustic intensity $I_{ac} \sim 1\text{--}100$ kW/cm² and frequency $\nu_{ac} \sim 0.1\text{--}1$ GHz. Due to the anomalously small interaction length between the acoustic and optical fields, possible applications of the effect are in THz spectroscopy and THz acousto-optic devices.

DOI: [10.1103/PhysRevB.81.245208](https://doi.org/10.1103/PhysRevB.81.245208)

PACS number(s): 71.36.+c, 43.35.+d

I. INTRODUCTION

Since the pioneering work by Kun Huang,¹ the physics of infrared polaritons associated with transverse-optical (TO) phonons has emerged as a well-established discipline. Recently, room-temperature polaritonics was implemented for processing and coherent control of the terahertz (THz) light field.^{2,3} In addition to conventional infrared spectroscopy and continuous-wave (cw) Raman-scattering experiments, broadband THz time-domain spectroscopy has been developed and successfully applied to characterize picosecond (ps) and sub-ps dynamics of infrared-active TO phonons⁴ and to visualize the polariton dispersion associated with these vibrational modes.⁵ Furthermore, the THz polariton spectra allow the study of unusual lattice dynamics, e.g., in ferroelectrics⁶ and negative thermal-expansion compounds.^{7,8} However, the spectrally resolved control of the electromagnetic field associated with far-infrared polaritons still remains a very challenging task of THz optics.

In this paper, we propose an acoustic modulation of TO-phonon polaritons in order to drastically change their optical response in the THz band. Phonon anharmonicity, which can be large in some dielectric and semiconductor materials and particularly strong for soft TO-phonon modes, leads to the coupling between a coherent (pumping) acoustic wave (AW) and infrared-active TO phonons. In this case one deals with an acoustically induced Autler-Townes effect, which gives rise to spectral gaps Δ_N in the THz polariton spectrum of AW-driven TO phonons, and is akin to the acoustical Stark effect for optically allowed excitons.^{9–14} The AW-induced gaps Δ_N , which open up in the polariton spectrum and develop with increasing acoustic intensity I_{ac} , are due to the N th-order resonant acoustic-phonon transitions within the polariton dispersion branches. These forbidden-energy gaps strongly modify the optical response of TO-phonon polaritons and make possible the effective AW-controlled manipulation of the THz field.

The spectrally resolved AW control of the THz field propagation can also be interpreted in terms of Bragg diffraction of far-infrared polaritons by the pumping AW: we analyze the use of phonon anharmonicity to create an acousti-

cally induced Bragg grating. In this case the contrast of the AW grating is dictated by the efficiency of the scattering channel “TO phonon \pm acoustic phonon (two acoustic phonons) \leftrightarrow TO phonon” for cubic (quartic) phonon anharmonicity. Thus the scattering of THz light is mediated and strongly enhanced by the TO-phonon resonance. This results in large acousto-optical nonlinearities and therefore in an anomalously short interaction length ℓ_{int} between the acoustic and optical fields needed for the formation of the Bragg replicas.

Possible applications of governing far-infrared polaritons by using an ultrasonic acoustic field include frequency-tunable THz detectors and filters, Bragg switchers, and frequency converters. The size of these devices would be much smaller than conventional acousto-optic equivalents, due to the rather small operating length scale, $\ell_{int} \sim 100$ μm .

In Sec. II, we discuss a model for far-infrared polaritons parametrically driven by the ultrasonic acoustic field, derive the macroscopic equations for resonantly coupled THz light field and polarization associated with TO phonons, and finally calculate the total Bragg reflectivity of TO-phonon polaritons. In Sec. III, the AW-induced response of THz polaritons in bulk CuCl (cubic phonon anharmonicity) and TlCl (quartic phonon anharmonicity) is modeled to illustrate the high efficiency of the effect and its potential for device applications. In Sec. IV, we discuss the results. A short summary of the work is given in Sec. V.

II. MODEL

The Hamiltonian of far-infrared polaritons coherently driven by a cw bulk acoustic wave $\{\mathbf{k}, \omega_{ac}(k)\}$ is given by

$$H = H_0 + \hbar \sum_{\mathbf{p}} [2\tilde{m}_4 I_{ac} b_{\mathbf{p}}^\dagger b_{\mathbf{p}} + (m_3 I_{ac}^{1/2} e^{-i\omega_{ac}t} b_{\mathbf{p}}^\dagger b_{\mathbf{p}-\mathbf{k}} + \text{H.c.}) + (m_4 I_{ac} e^{-2i\omega_{ac}t} b_{\mathbf{p}}^\dagger b_{\mathbf{p}-2\mathbf{k}} + \text{H.c.})] \quad (1)$$

with H_0 the conventional polariton Hamiltonian of infrared-active TO phonons,¹⁵ $b_{\mathbf{p}}$ the TO-phonon operator, $\omega_{ac} = 2\pi\nu_{ac} = v_s k$, v_s the sound velocity, and m_3 (m_4 and \tilde{m}_4) the matrix element associated with cubic (quartic) anharmonicity.

ity. The macroscopic equations, which describe the control of THz polaritons by applying the acoustic field of an arbitrary profile, $I_{ac}=I_{ac}(\mathbf{r},t)$, are

$$\left[\frac{\epsilon_b}{c^2} \frac{\partial^2}{\partial t^2} - \nabla^2 \right] \mathbf{E}(\mathbf{r},t) = - \frac{4\pi}{c^2} \frac{\partial^2}{\partial t^2} \mathbf{P}(\mathbf{r},t), \quad (2)$$

$$\left[\frac{\partial^2}{\partial t^2} + 2\gamma_{TO} \frac{\partial}{\partial t} + \Omega_{TO}^2 + 4\Omega_{TO}\tilde{m}_4 I_{ac}(\mathbf{r},t) + 4\Omega_{TO}m_3 I_{ac}^{1/2}(\mathbf{r},t)\cos(\omega_{ac}t - \mathbf{k}\mathbf{r}) + 4\Omega_{TO}m_4 I_{ac}(\mathbf{r},t)\cos(2\omega_{ac}t - 2\mathbf{k}\mathbf{r}) \right] \mathbf{P}(\mathbf{r},t) = \frac{\epsilon_b}{4\pi} \Omega_R^2 \mathbf{E}(\mathbf{r},t), \quad (3)$$

where \mathbf{E} and \mathbf{P} stand for the light field and TO-phonon polarization, respectively, Ω_{TO} is the TO-phonon frequency, Ω_R is the polariton Rabi frequency, ϵ_b is the background dielectric constant in the infrared, and γ_{TO} is the damping rate of TO phonons, mainly due to their decay into short-wavelength acoustic phonons. Equations (2) and (3) refer to simple cubic lattices with spatially isotropic long-wavelength anharmonicity and optical response. For cw acoustic excitations, when $I_{ac}(\mathbf{r},t)=I_{ac}=\text{const}$, Eqs. (2) and (3) yield the same quasienergy spectrum as that of the quadratic Hamiltonian (1). If $I_{ac}=0$, Eqs. (2) and (3) reduce to the standard TO-phonon polariton equations.¹ The fourth term on the left-hand side (lhs) of the polarization Eq. (3) yields a Stark shift of the TO-phonon frequency, which is $\propto I_{ac}$ and is associated with the quartic phonon nonlinearity. The last two terms on the lhs of Eq. (3) give rise to the Bragg spectrum of TO-phonon polaritons driven by the AW.

In Eqs. (1) and (3), the matrix elements $m_{3,4}$ and \tilde{m}_4 are given by

$$m_3 = 6 \left(\frac{v_0}{\hbar^3 v_s^2 k} \right)^{1/2} V_3(\mathbf{k}, \mathbf{p} - \mathbf{k}, -\mathbf{p}),$$

$$m_4 = 12 \left(\frac{v_0}{\hbar^2 v_s^2 k} \right) [V_4(\mathbf{k}, \mathbf{k}, \mathbf{p} - 2\mathbf{k}, -\mathbf{p}) + V_4(\mathbf{k}, \mathbf{k}, -\mathbf{p}, \mathbf{p} - 2\mathbf{k})],$$

$$\tilde{m}_4 = 24 \left(\frac{v_0}{\hbar^2 v_s^2 k} \right) V_4(\mathbf{k}, -\mathbf{k}, \mathbf{p}, -\mathbf{p}), \quad (4)$$

where v_0 is a volume of the primitive cell and

$$V_3(\mathbf{k}, \mathbf{p} - \mathbf{k}, -\mathbf{p}) = \frac{1}{6} \left(\frac{\hbar^3}{8v_s k \Omega_{TO}^2} \right)^{1/2} \Phi^{(3)}(\mathbf{k}, \mathbf{p} - \mathbf{k}, -\mathbf{p}), \quad (5)$$

$$V_4(\mathbf{k}, -\mathbf{k}, \mathbf{p}, -\mathbf{p}) = \frac{1}{24} \left(\frac{\hbar^2}{4v_s k \Omega_{TO}} \right) \Phi^{(4)}(\mathbf{k}, -\mathbf{k}, \mathbf{p}, -\mathbf{p}). \quad (6)$$

Here, $\Phi^{(3)}$ ($\Phi^{(4)}$) is proportional to the Fourier transform of the third-order (fourth-order) spatial derivative of the interatomic potential. The explicit formulas for $\Phi^{(3,4)}$ are given, e.g., in Refs. 16 and 17.

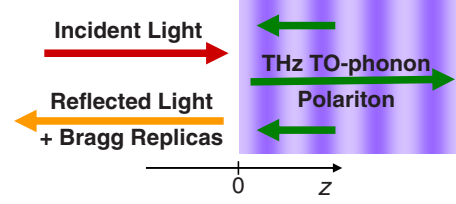


FIG. 1. (Color online) Schematic of optical excitation and backward Bragg scattering of an acoustically driven THz polariton. Vertical stripes symbolize the propagating bulk acoustic wave.

In the long-wavelength limit $k, p \ll 1/a_0$ (a_0 is the lattice constant), relevant to the optics of TO-phonon polaritons, $\Phi^{(3,4)}$ are well approximated by $\Phi^{(3)}=(ka_0)C_3$ and $\Phi^{(4)}=(ka_0)^2 C_4$.¹⁸ The anharmonicity constants $C_{3,4}$ can either be calculated by using modern *ab initio* methods^{19,20} or evaluated from experimental data available for some anharmonic crystals.^{21–25} The above approximation of $\Phi^{(3,4)}$ also leads to the k -independent matrix elements m_3 and $\tilde{m}_4=m_4$ in Eqs. (1) and (3).

Recently, the third-order coupling constant V_3 was inferred for some zinc-blende-type semiconductors (GaP, CuCl, CuBr, and β -ZnS) which exhibit strong and dominant cubic anharmonicity.^{21–24} The used experimental data refers to the decay of a long-wavelength TO phonon into short-wavelength longitudinal-acoustic and transverse-acoustic (TA) phonons. To adapt the inferred values of V_3 to m_3 in Eqs. (1)–(3), we use the Leibfried-Ludwig approximation²⁶ according to which $\Phi^{(3)}$ in Eq. (5) is the same for the whole Brillouin zone. The parameter $m_3 I_{ac}^{1/2}$, which controls cubic-anharmonicity-mediated manipulation of THz polaritons by means of a bulk TA wave, is evaluated for CuCl as $\hbar m_3 I_{ac}^{1/2} \approx 0.26$ meV (63 GHz) for $I_{ac}=1$ kW/cm². In thallium halides (TlCl and TlBr), quartic anharmonicity is dominant with positive values of V_4 . With the Leibfried-Ludwig approximation of Eq. (6), one can evaluate the control parameter $m_4 I_{ac}$ from the available experimental data on the real part of the TO-phonon self-energy.²⁵ For TlCl pumped by a bulk TA wave we get $\hbar m_4 I_{ac} \approx 0.4$ meV (97 GHz) for $I_{ac}=100$ kW/cm².

We examine the optical response of an acoustically driven TO-phonon polariton in a one-dimensional geometry, when a semiconductor occupies the half space $z>0$, and a normally incident light field of frequency ω induces a THz polariton propagating collinearly to the pumping AW (see Fig. 1). In this case, apart from reflectivity at the same frequency ω , down-converted Bragg replicas at $\omega+n\omega_{ac}$ ($n=-1, -2, \dots$) arise in the reflection spectrum, due to acoustically induced backward scattering of the polariton. In order to calculate the multiple Bragg replicas, we develop an approach more advanced than that used in conventional acousto-optics. For the latter, the acousto-optical susceptibilities are so weak that usually only one Bragg replica $n=+1$ or -1 is seen. In contrast, the TO-phonon resonance mediates and considerably enhances the coupling between the optical and acoustic fields, so that generally one has to take into account the whole series of the Bragg replicas and multiphonon transitions, thus treating the problem nonperturbatively.

The quasienergy polariton spectrum $\omega=\omega(p)$, calculated for real-valued p (quasiparticle solution) by solving Eqs. (2)

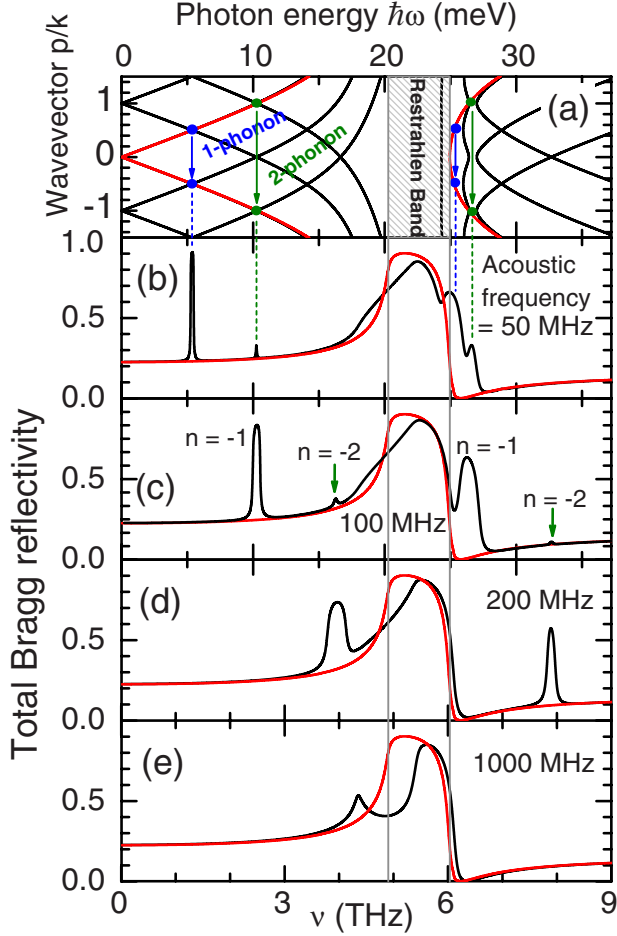


FIG. 2. (Color online) (a) The dispersion $\omega = \omega(p)$ of THz polaritons in CuCl driven by the bulk TA wave of $\nu_{\text{ac}} = 50$ MHz, black lines, and the bare polariton spectrum, red (dark gray) lines. The wave vector p is normalized to the acoustic wave vector k . The arrows highlight the N -TA-phonon resonant coupling between the polariton states ($N=1,2$). [(b)–(e)] The calculated total Bragg reflectivity (black lines), $R = \sum_n |r_n|^2$, against the light frequency $\nu = \omega/(2\pi)$ for $\nu_{\text{ac}} = 50$ MHz, 100 MHz, 200 MHz, and 1 GHz, respectively. The bare polariton reflectivity is shown by the red (dark gray) lines. The Bragg signals labeled in (c) as $n=-1$ and $n=-2$ are mainly due to $|r_{-1}|^2$ and $|r_{-2}|^2$, respectively. The acoustic intensity $I_{\text{ac}} = 25$ kW/cm².

and (3) with $m_4=0$, is plotted in Fig. 2(a) for CuCl parametrically driven by the TA wave of frequency $\nu_{\text{ac}} = 50$ MHz and constant intensity $I_{\text{ac}} = 25$ kW/cm². The spectrum, which arises from spatial and temporal modulation of the crystal lattice, can be interpreted in terms of the Brillouin-zone picture, with acoustically induced energy gaps $\Delta_N \propto I_{\text{ac}}^{N/2}$ due to the N -phonon resonant transitions within the polariton dispersion branches. The spectral positions of the transitions are indicated in Fig. 2(a) by the vertical arrows. For the frequency scale used in Fig. 2(a), only the gaps $\Delta_{N=1}$ and $\Delta_{N=2}$ in the upper polariton branch are clearly seen.

From the air side, $z < 0$ (see Fig. 1), the light field is given by

TABLE I. Parameters of bulk CuCl and TlCl used in the numerical calculations.

	CuCl	TlCl
$\hbar\Omega_{\text{TO}}$ (meV)	20.28	7.81
$\hbar\Omega_{\text{R}}$ (meV)	14.53	17.97
$\hbar\gamma_{\text{TO}}$ (meV)	0.20	0.92
v_s (10^5 cm/s)	2.02	2.19
$\hbar m_3$ (10^{-12} meV ^{1/2} cm s ^{1/2})	0.10	0
$\hbar m_4$ (10^{-27} cm ² s)	0	0.64

$$E(z < 0, t) = e^{iq_0 z} e^{-i\omega t} + \sum_n r_n e^{-iq_n z} e^{-i(\omega + n\omega_{\text{ac}})t}, \quad (7)$$

where $q_n = (\omega + n\omega_{\text{ac}})/c$ with $-n_{\text{max}} \leq n \leq n_{\text{max}}$ (we proceed up to $n_{\text{max}} = 60$) and r_n stands for the amplitude of the outgoing Bragg replica n normalized to the unity amplitude of the incoming light wave. The electric field propagating in the crystal ($z > 0$) is

$$E(z > 0, t) = \sum_{n,j} A_j E_{nj} e^{i(p_j + nk)z - i(\omega + n\omega_{\text{ac}})t}. \quad (8)$$

Here, $p_j = p_j(\omega)$ is the wave vector associated with the quasienergy dispersion branch j ($-n_{\text{max}} \leq j \leq n_{\text{max}}$) of the acoustically driven polariton, E_{nj} are the corresponding normalized eigenvectors, and A_j are the eigenmode amplitudes. Both $p_j = p_j(\omega)$ and E_{nj} are the forced-harmonic solutions of Eqs. (2) and (3) for real-valued frequency ω . The exponential on the right-hand side of Eq. (8) as well as the basic relationships $p_{j+s}(\omega) = p_j(\omega - s\omega_{\text{ac}}) + sk$ and $E_{n,j+s}(\omega) = E_{n+s,j}(\omega - s\omega_{\text{ac}})$, with integer s , reflect the acoustic wave vector and frequency translational invariance of the quasienergy spectrum. The Maxwellian boundary conditions at $z=0$ together with Eqs. (7) and (8) yield,

$$\delta_{n,0} + r_n = \sum_j A_j E_{nj}, \quad \delta_{n,0} - r_n = \sum_j A_j E_{nj} \frac{p_j + nk}{q_n}. \quad (9)$$

The above set of $2(2n_{\text{max}} + 1)$ linear equations determines r_n and A_j .

III. NUMERICAL MODELING

In this section, by solving numerically Eqs. (2), (3), and (9), we model the terahertz response of acoustically pumped copper chloride and thallium chloride crystals. For the first (second) compound, we set $m_4 = \tilde{m}_4 = 0$ ($m_3 = 0$) in Eq. (3), according to the relative strength of the cubic and quartic anharmonicity coefficients in CuCl (TlCl). Table I summarizes values of the parameters used in numerical simulations.

A. Acoustically driven THz polaritons in bulk CuCl

In Figs. 2(b)–2(e), we compare the calculated total Bragg reflectivity, $R = R(\omega) = \sum_n |r_n|^2$ (black solid lines), with the reflectivity of the acoustically unperturbed THz polariton, $R^{(0)} = R^{(0)}(\omega)$ [red (dark gray) solid lines]. The sharp spikes in the Bragg spectrum of the acoustically driven CuCl crystal

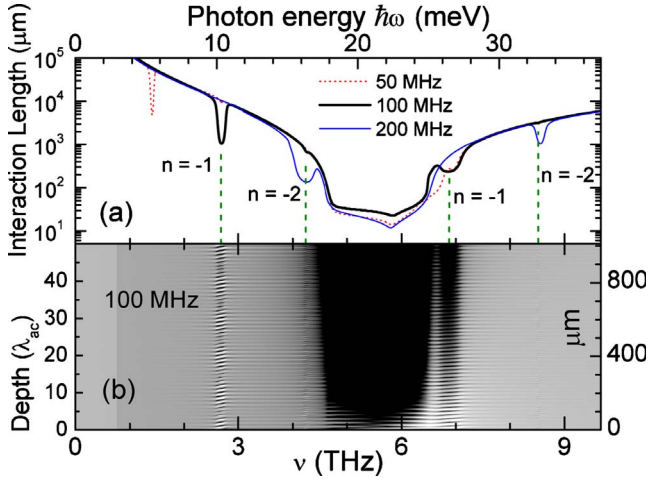


FIG. 3. (Color online) (a) The interaction length between the THz polariton and TA pumping wave in CuCl, $\ell_{\text{int}} = \ell_{\text{int}}(\omega)$, calculated for $I_{\text{ac}} = 25 \text{ kW/cm}^2$ and $\nu_{\text{ac}} = 50, 100,$ and 200 MHz . (b) The electric field profile $|E(z > 0, \omega)|^2$ evaluated for $\nu_{\text{ac}} = 100 \text{ MHz}$ ($\lambda_{\text{ac}} = 20.2 \text{ }\mu\text{m}$). The gray-black color scale is logarithmic with black color corresponding to $E \rightarrow 0$.

are clearly seen for the one-TA-phonon and two-TA-phonon transitions, both for the upper-polariton (UP) and lower-polariton (LP) branches [see Fig. 2(a) against Fig. 2(b)]. For $\nu_{\text{ac}} \sim 30\text{--}300 \text{ MHz}$, the backward scattered Bragg replica $|r_{-1}|^2$ peaks at the energy of the one-phonon transition and is highly efficient, with $|r_{-1}|^2/R \sim 50\text{--}70 \%$. The peak position and its strength are effectively tunable by changing the frequency and intensity of the AW [see Figs. 2(b)–2(d)]. This can be used for the frequency down conversion by $\omega_{\text{ac}} = 2\pi\nu_{\text{ac}}$ of the optically induced THz polariton and thus of the incident light field. Generally, the backward Bragg scattering signals $|r_n|^2 \propto I_{\text{ac}}^{|n|}$ ($n < 0$) peak at the spectral position of the gaps $\Delta_{N \leq |n|}$, i.e., for the light frequency $\omega = \omega_N$ which satisfies the resonant Bragg condition $p_{j=0}(\omega_N) \approx Nk/2$ with $N = 1, 2, \dots, |n|$.

The Bragg signal $n=0$ appears as the AW-induced change in the reflectivity at incident frequency ω , $|r_0(\omega)|^2 - R^{(0)}(\omega)$. The strength of the $n=0$ signal sharply increases with decreasing detuning $|\omega_{N=1} - \Omega_{\text{TO}}|$ from the TO-phonon resonance so that $|r_0|^2 - R^{(0)}$ becomes dominant over $|r_{-1}|^2$. For $\nu_{\text{ac}} \gtrsim 1 \text{ GHz}$, when the one-acoustic-phonon transition within the LP branches occurs very close to Ω_{TO} , the AW-induced change in the reflectivity [see Fig. 2(e)] is completely determined by the $n=0$ replica and has no ν_{ac} -down-converted frequency components. Thus, this operating mode can be used for TO-phonon polariton deflectors and acoustically controlled THz filters.

The interaction length $\ell_{\text{int}} = \ell_{\text{int}}(\omega)$ required for the formation of the Bragg signals and thus for AW control of the THz light field is plotted in Fig. 3(a) for various ν_{ac} . The sharp troughs at $\omega = \omega_{N=1}$ and $\omega_{N=2}$ in the $\ell_{\text{int}} = \ell_{\text{int}}(\omega)$ profile are due to the $n=-1$ and -2 Bragg replicas [see Fig. 3(a)]. Figure 3(b) shows the light field distribution associated with the optically induced THz polariton in the acoustically driven CuCl crystal. Apart from the broad black band [see Fig. 3(b)], which corresponds to the Reststrahlen band with rather

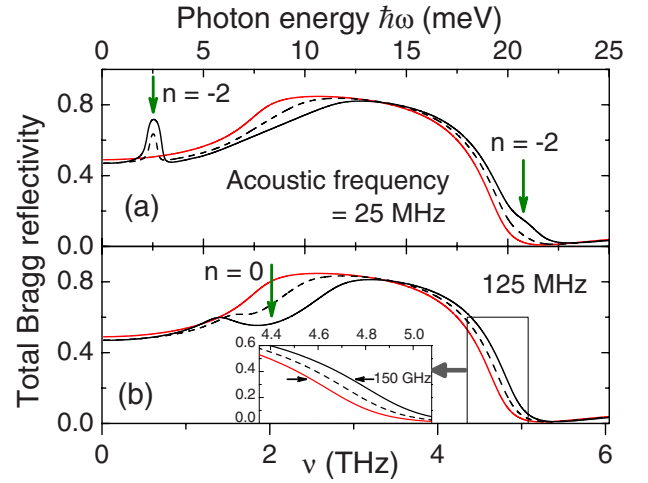


FIG. 4. (Color online) The total Bragg reflectivity $R = R(\omega)$ of a TlCl crystal driven by the TA wave of frequency (a) $\nu_{\text{ac}} = 25 \text{ MHz}$ and (b) 125 MHz , $I_{\text{ac}} = 100 \text{ kW/cm}^2$ (black dotted lines) and 200 kW/cm^2 (black solid lines). The acoustically unperturbed THz spectrum $R^{(0)} = R^{(0)}(\omega)$ is shown by the red (dark gray) lines. Inset: the acoustically induced Stark shift of the TO-phonon line.

weak penetration of the light field into the crystal, the narrow stripes of alternating color illustrate the formation of the Bragg replicas. The interaction length for the $n=-1$ replica at its resonant frequency $\omega = \omega_{N=1}$ is given by

$$\ell_{\text{int}} = \frac{\hbar kc^2}{4m_3 I_{\text{ac}}^{1/2} \epsilon_b} \frac{(\omega_{N=1}^2 - \Omega_{\text{TO}}^2)^2}{\omega_{N=1}^2 \Omega_{\text{TO}} \Omega_R^2}. \quad (10)$$

Equation (10), which is valid for $|\Omega_{\text{TO}} - \omega_{N=1}| \gg \gamma_{\text{TO}}$ and $\ell_{\text{int}} k \gg 1$, shows the resonant decrease in $\ell_{\text{int}} \propto 1/\sqrt{I_{\text{ac}}}$ with decreasing frequency detuning from the TO-phonon resonance. In this case the interaction between the light field and pumping AW is mediated by the TO-phonon resonance, giving rise to ℓ_{int} of only a few tens of acoustic wavelength λ_{ac} (see Fig. 3). This is in sharp contrast with conventional acousto-optics where $\ell_{\text{int}} \sim 10^3\text{--}10^4 \lambda_{\text{ac}}$ for the same operating I_{ac} .

B. Acoustically driven THz polaritons in bulk TlCl

The calculated room-temperature reflectivity $R = R(\omega)$ of a TlCl crystal pumped by the TA wave of frequency $\nu_{\text{ac}} = 25 \text{ MHz}$ and 125 MHz is plotted in Figs. 4(a) and 4(b), respectively. In this case, in Eqs. (1) and (3) we put $m_3 = 0$, and therefore only even-order TA-phonon-assisted transitions occur. The Bragg signals $n=-2$, due to $|r_{-2}|^2 \propto I_{\text{ac}}^2$, are indicated in Fig. 4(a) by arrows, for the transitions within the LP and UP branches, respectively. Similarly to the previous case (CuCl), for the resonant frequency $\omega_{N=2}$ close to Ω_{TO} the AW-induced change in R , $\Delta R = R - R^{(0)} \sim I_{\text{ac}}^2$ [see Fig. 4(b)], is mainly due to the $n=0$ Bragg replica. The quartic nonlinearity leads to the Stark blueshift by $2m_4 I_{\text{ac}}$ of the TO-phonon frequency, according to Eqs. (1) and (3), as is clearly seen in Figs. 4(a) and 4(b). The Stark shift $\sim 0.1\text{--}0.2 \text{ THz}$ has a rather sharp contrast on the blue side of the THz reflectivity

[see inset of Fig. 4(b)]. This can be used in device applications, e.g., for frequency tunable THz filters and deflectors.

IV. DISCUSSION

The third- and fourth-order anharmonic nonlinearities tend to cancel each other^{17,23} so that the values of m_3 (CuCl) and m_4 (TlCl) we have inferred from the experimental data are in the lowest limit of their actual values. The proposed acoustic modulation of THz polaritons generally allow us, by comparing $n=-1$ and $n=-2$ Bragg replicas evaluated with Eqs. (2), (3), and (9), to distinguish the two nonlinearities as well as to analyze interference between the cubic and quartic anharmonic coefficients. The latter process occurs, e.g., for soft TO phonons in ferroelectric LiTaO₃ and LiNbO₃.

Within the used nonperturbative approach, each Bragg replica n integrates all $n+s-s$ TA-phonon transitions with $s \leq n_{\max}$: with increasing I_{ac} the bare n -phonon transitions become dressed by higher-order processes when $n+s$ phonons are emitted and s phonons absorbed. For the $n=-1$ replica shown in Fig. 2(b), e.g., the multiphonon transitions $-1+1-1$, $-1+2-2$, etc., account for about 90% of $|r_{-1}|^2$. For $\nu_{\text{ac}} \geq 1$ GHz [see Fig. 2(e)], the dominant contribution to $|r_0|^2 - R^{(0)}$ stems from $-s+s$ multi-TA-phonon transitions with $s > 1$.

The acoustically induced modulation of far-infrared polaritons has to be particularly strong for ferroelectric soft TO phonons (e.g., in LiTaO₃ and LiNbO₃,⁶ and bismuth titanate⁵). In this case, a multiwell local potential for the displacive ferroelectric mode has a considerable low-wave-vector component and therefore yields large values of V_3 and V_4 . Very far-infrared optical phonons (2–10 meV) in zirconium tungstate (ZrW₂O₈) indicate anomalously high anharmonicity.^{7,8} The normal modes associated with soft TO phonons in this negative thermal-expansion compound are a mixture of librational and translational motion. The latter strongly couples with acoustic phonons giving rise, as we foresee, to manipulation of the THz polaritons by using ultrasound waves of modest I_{ac} .²⁷

In accordance with Eq. (4), m_3 and m_4 scale to the sound velocity as $v_s^{-3/2}$ and v_s^{-3} , respectively. As a result, the use of a surface AW in order to control the propagation of THz polaritons considerably reduces the operating acoustic intensity I_{ac} : $v_s = v_{\text{SAW}}$ is usually by about 20% less than $v_s = v_{\text{TA}}$.

The realistic values of the damping constant, $\hbar\gamma_{\text{TO}} = 0.2$ meV for CuCl at $T=5-10$ K (Refs. 21 and 23) and

$\hbar\gamma_{\text{TO}} = 0.9$ meV for TlCl at room temperature,²⁵ are used in our numerical simulations. Note that γ_{TO} is rather weakly temperature dependent, e.g., roughly doubling its value for CuCl with increasing temperature from cryogenic values to the room one. In all the materials mentioned in the paper, the polariton effect associated with TO phonons persists at room temperature. This is because the Rabi frequency of THz polaritons, $\hbar\Omega_{\text{R}} \sim 10$ meV, is much larger than the damping constant, which even for soft TO-phonon modes is usually $\hbar\gamma_{\text{TO}} \sim 0.5-1$ meV only.

V. SUMMARY

In this paper we have proposed, theoretically described, and numerically modeled the THz response of far-infrared polaritons parametrically driven by a coherent acoustic field. The cubic and quartic phonon anharmonicity processes give rise to an acoustically induced Bragg grating. In this case, the TO-phonon resonance mediates and strongly enhances the acousto-optical nonlinearity leading to the anomalously small interaction length $\ell_{\text{int}} \sim 100$ μm between the optical and acoustic fields, which is required for the formation of the THz response (Bragg replicas). The main results of the work are: (i) the macroscopic Eqs. (2) and (3), which describe spatially temporal or wave-vector-frequency effective control of far-infrared polaritons and THz light associated with them by applying the acoustic field. (ii) The nonperturbative approach, based on Eqs. (7)–(9), to calculate the total Bragg reflectivity of TO-phonon polaritons modulated by the ultrasonic acoustic wave. (iii) The illustration of the high efficiency of the proposed effect by numerical modeling of the THz response of bulk CuCl and TlCl pumped by the coherent acoustic field. (iv) The large potential of the effect for device applications: the small interaction length between the THz light and subgigahertz acoustic field would potentially lead to a new family of THz microdevices, such as frequency-tunable THz detectors and filters, Bragg switchers, and frequency converters.

ACKNOWLEDGMENTS

We thank S. G. Tikhodeev, D. R. Khokhlov, P. Mauskopf, and R. Zimmermann for valuable discussions. This work was supported by RS (Grant No. JP0766306), EPSRC and WIMCS.

¹K. Huang, *Nature (London)* **167**, 779 (1951); *Proc. R. Soc. London, Ser. A* **208**, 352 (1951).

²N. S. Stoyanov, D. W. Ward, T. Feurer, and K. A. Nelson, *Nature Mater.* **1**, 95 (2002).

³T. Feurer, J. C. Vaughan, and K. A. Nelson, *Science* **299**, 374 (2003).

⁴P. Y. Han and X.-C. Zhang, *Meas. Sci. Technol.* **12**, 1747 (2001).

⁵S. Kojima, N. Tsumura, M. W. Takeda, and S. Nishizawa, *Phys. Rev. B* **67**, 035102 (2003).

⁶H. J. Bakker, S. Hunsche, and H. Kurz, *Rev. Mod. Phys.* **70**, 523 (1998).

⁷J. N. Hancock, C. Turpen, Z. Schlesinger, G. R. Kowach, and A. P. Ramirez, *Phys. Rev. Lett.* **93**, 225501 (2004).

⁸S. L. Chaplot, *Curr. Sci.* **88**, 347 (2005).

⁹A. L. Ivanov and P. B. Littlewood, *Phys. Rev. Lett.* **87**, 136403 (2001).

¹⁰K. Cho, K. Okumoto, N. I. Nikolaev, and A. L. Ivanov, *Phys. Rev. Lett.* **94**, 226406 (2005).

- ¹¹A. L. Ivanov, *Phys. Status Solidi A* **202**, 2657 (2005).
- ¹²M. M. de Lima, R. Hey, P. V. Santos, and A. Cantarero, *Phys. Rev. Lett.* **94**, 126805 (2005).
- ¹³M. M. de Lima, M. van der Poel, P. V. Santos, and J. M. Hvam, *Phys. Rev. Lett.* **97**, 045501 (2006).
- ¹⁴A. L. Ivanov, in *Problems of Condensed Matter Physics*, edited by A. L. Ivanov and S. G. Tikhodeev (Oxford University Press, Oxford, 2008), pp. 301–322.
- ¹⁵V. Romero-Rochín, R. M. Koehl, C. J. Brennan, and K. A. Nelson, *J. Chem. Phys.* **111**, 3559 (1999).
- ¹⁶A. A. Maradudin and A. E. Fein, *Phys. Rev.* **128**, 2589 (1962).
- ¹⁷R. A. Cowley, *Rep. Prog. Phys.* **31**, 123 (1968).
- ¹⁸G. P. Srivastava, *The Physics of Phonons* (Taylor & Francis, New York, 1990).
- ¹⁹A. Debernardi, S. Baroni, and E. Molinari, *Phys. Rev. Lett.* **75**, 1819 (1995).
- ²⁰G. Deinzer, M. Schmitt, A. P. Mayer, and D. Strauch, *Phys. Rev. B* **69**, 014304 (2004).
- ²¹C. Ulrich, A. Göbel, K. Syassen, and M. Cardona, *Phys. Rev. Lett.* **82**, 351 (1999).
- ²²F. Widulle, T. Ruf, A. Göbel, E. Schönherr, and M. Cardona, *Phys. Rev. Lett.* **82**, 5281 (1999).
- ²³M. Cardona and T. Ruf, *Solid State Commun.* **117**, 201 (2001).
- ²⁴J. Serrano, A. Cantarero, M. Cardona, N. Garro, R. Lauck, R. E. Tallman, T. M. Ritter, and B. A. Weinstein, *Phys. Rev. B* **69**, 014301 (2004).
- ²⁵R. P. Lowndes, *Phys. Rev. Lett.* **27**, 1134 (1971); *Phys. Rev. B* **6**, 1490 (1972).
- ²⁶G. Leibfried and W. Ludwig, in *Solid State Physics*, edited by F. Seitz and D. Turnbull (Academic Press, New York, 1961), Vol. 12.
- ²⁷The operating acoustic intensities used in the simulations of bulk CuCl and TiCl driven by a TA wave are similar to those applied to a GaAs-based microcavity (MC) in the experiments (Refs. 12 and 13). The latter study deals with the acoustical Stark effect for MC polaritons. Our recent evaluations yield a much smaller operating intensity, $I_{ac} \approx 1-10$ kW/cm², needed for the effective manipulation of TO-phonon polaritons in LiNbO₃ driven by a bulk TA wave. For ZrW₂O₈, we anticipate still further reduction in the operating acoustic intensities toward a subkilowatt per square centimeter scale.